Composites Part A 134 (2020) 105910

Contents lists available at ScienceDirect

Composites Part A

journal homepage: www.elsevier.com/locate/compositesa

Facile synthesis of substrate supported ultrathin two-dimensional cobalt-based metal organic frameworks nanoflakes

Yu Fu[a], Hanmo Zhou[a], Sha Yin[b,*], Limin Zhou[a,*]

[a] Department of Mechanical Engineering, The Hong Kong Polytechnic University, Hung Hom, Kowloon, Hong Kong, China
[b] Department of Automotive Engineering, School of Transportation Science and Engineering, Beihang University, Beijing 100191, China

ARTICLE INFO

Keywords:
A. Carbon cloth
A. Polymer-based composites
Metal organic frameworks
Ultrathin nanoflakes

ABSTRACT

The synthesis of substrate-supported metal–organic-framework (MOF) nanoflakes has become a research hotspot due to its attractive use as precursors to prepare metal (oxide)/carbon nanocomposites for the applications of catalysis and energy storage. This work reports facile synthesis of a newly-structured ultrathin Cobalt-based MOF (Co-MOF) nanoflakes on carbon cloth (CC). Through changing reaction time and reactant concentration, Co-MOF morphologies can be easily controlled, which paves ways for controllable fabrication of ultrathin Co_3O_4 nanoflakes on CC based on the phase transformation from Co-MOF to Co_3O_4. Meanwhile, the good compatibility of this mechanically strong Co-MOF with polymer inspires us to tailor CC@Co_3O_4 from the perspective of polymer-based researches, such as polymer-based catalysts and solid state batteries using a solid state polymer electrolyte. Therefore, this study not only enriches the family of MOFs but lays foundations for fabrication of next-generation CC-reinforced polymer composites for multifunctional applications such as catalysis and energy storage.

1. Introduction

The synthesis of nanoscale metal organic frameworks [1–3] (MOFs) has become a research hotspot due to its attractive use as precursors to prepare various metal (oxide)/porous carbon nanocomposite compounds for energy storage and catalytic applications, etc. by pyrolysis or chemical methods [4]. Despite the fact that MOF and its derivatives possess tremendous advantages in various fields, their practical applications are hampered because powdered MOFs and its derivatives are typically poorly processable [5]. To take an example, when used for energy storage devices, bulk powder MOFs and its derivatives require the use of polymer binders and conductive additives in the assembly of electrodes, leading to fewer active sites, loss of active materials and enlarged interfacial resistances, which limit electrochemical properties. Therefore, stable MOF coatings on various substrates are needed for practical applications.

Among these supported MOF coatings, nanoscale MOFs with nanoflake morphology have caught wide attention from scientists in the fields of energy storage [6], catalysis [7] and sensor [8], etc. due to their diversified structures, tunable chemical functionalities, large surface area and ultrathin thicknesses. Furthermore, due to low tendency of MOF nanoflakes to aggregate during pyrolysis, the obtained flake-structured MOF-derivatives are blessed with a great deal of accessible active metal sites and fast electron transfer and thus have high potential to be used as electrodes [9] or catalysts [10]. Especially, ultrathinning nanoflakes into nanometre thicknesses has been reported to be a very effective strategy to acquire high-performance electrocatalysts [11] and battery electrodes [12]. Therefore, fabrication of substrate-based ultrathin nanoflakes attracts enormous research interest. Conventionally, preparation of MOF nanoflakes is mainly based on two kinds of methods [13]. One method is a top-down growth strategy in which exfoliation of bulk-layered MOFs occurs. However, structural deterioration and morphological fragmentation inevitably occur in this method, meanwhile, only a low yield (normally < 15%) can be obtained and separating nanoflakes from bulk materials is very complicated. Furthermore, a top down method has low applicability for substrate supported MOF growth. Therefore, a bottom-up method [14] is more promising to synthesize substrate supported high-quality MOF nanoflakes. Attributed to the high potential of Co_3O_4 for the applications of catalysis and energy storage [15], there have been many reports on carbon cloth (CC)/nickel foam supported cobalt-based MOF-derived Co_3O_4 up to now [16–18]. However, the thickness of most of the previously reported Co-MOF nanoflakes is not less than 100 nm. Reports on ultrathin nanoflakes are quite rare. Even though discrete nanoflakes with the thickness of ~2 nm were synthesized in solvent [19], the two-step synthesis procedures were complicated and the feasibility of the

* Corresponding authors.
E-mail addresses: shayin@buaa.edu.cn (S. Yin), mmlmzhou@polyu.edu.hk (L. Zhou).

https://doi.org/10.1016/j.compositesa.2020.105910
Received 8 December 2019; Received in revised form 13 April 2020; Accepted 18 April 2020
Available online 20 April 2020
1359-835X/

growth of these ultrathin Co-MOF nanoflakes on substrates was not confirmed. Therefore, synthesis of substrate supported ultrathin MOF nanoflakes in an easy way is still in high demand.

Herein, through replacing water solvent with methanol and applying an appropriate reactants ratio, facile synthesis of homogeneously distributed Co-MOF nanoflakes with a thickness of ~8 nm on hydrophilic CC is demonstrated (CC@Co-MOF) instead of thick Co-MOF nanoflakes when water is used as solvent. Effects of reaction time and reactants concentration on Co-MOF morphology have been explored and morphologies of the CC@Co-MOF can be easily controlled, which paves the way for the fabrication of morphology-controllable CC@Co_3O_4 nanoflakes in future. Meanwhile, good compatibility of ultrathin Co-MOF nanoflakes and polymer has also been demonstrated, which further enables exploration of CC@Co_3O_4 nanoflakes for the applications of polymer-based Co_3O_4 catalysts and batteries utilizing a solid-state polymer electrolyte. Therefore, this study not only demonstrates facile synthesis of a newly designed ultrathin MOF nanoflakes supported on CC, but puts forward a high possibility of obtaining CC@Co_3O_4 nanoflakes reinforced polymer composites with promising properties for catalysis and energy storage, which can open up new possibilities for obtaining multifunctional CC reinforced polymer composites.

2. Experimental section

2.1. Materials

CC (3k CFs, FAW 200 gsm, plain weave) was acquired from TEI Composite (Taiwan) and thermally treated at 450 °C for 1 h in an Ar_2 atmosphere to remove the sizing. $Co(NO_3)_2{\cdot}6H_2O$, 2-methylimidazole, $Zn(NO_3)_2{\cdot}6H_2O$, Anhydrous $FeCl_3$, 1,4-Benzenedicarboxylic acid, were purchased from Sigma-Aldrich (USA). Fuming sulfuric acid (H_2SO_4), nitric acid (HNO_3), methanol and N,N′-dimethylformamide (DMF) were obtained from VWR International (Hong Kong). WS 105 epoxy resin matrix and WS 209 hardener were provided by High Gain Industrial, Co., Ltd. (Hong Kong). All chemical reagents and solvents were used as received.

2.2. Fabrication of CC@Co-MOF

CC@Co-MOF was synthesized as follows. CC was pretreated with concentrated H_2SO_4/HNO_3 (molar ratio = 3:1) for 45 min and cleaned with deionized water several times before further use. The obtained CC, denoted as CC-COOH, was then used to grow Co-MOF, Zn-MOF and Fe-MOF. In a typical procedure for Co-MOF growth, $Co(NO_3)_2{\cdot}6H_2O$ (9.313 g) and 2-methylimidazole (1.3135 g) in a molar ratio of 2:1 were separately dissolved in two beakers of methanol (2 × 100 mL) with continuous stirring for 10 min at room temperature. The $Co(NO_3)_2{\cdot}6H_2O$ methanol solution was then quickly poured into the 2-methylimidazole methanol solution. After homogeneous blending for 5 min, the mixed solution was poured into Teflon-lined autoclave with a CC-COOH. After reaction at 90 °C for 24 h, the CC-COOH was removed and washed with methanol three times and left in an oven overnight at 60 °C. Similarly, in order to grow Zn-MOF and Fe-MOF, $Zn(NO_3)_2{\cdot}6H_2O$/2-methylimidazole (9.520 g/2.392 g) and $FeCl_3$/1,4-Benzenedicarboxylic acid (5.190 g/5.316 g) inorganic–organic linker pairs were dissolved in DMF (200 mL) at room temperature, respectively. Afterwards, CC-COOHs were immersed into two kinds of solution and the temperatures were maintained at 150 °C for 15 h and at 140 °C for 24 h, respectively. After reaction, the CC-COOHs were removed and washed with DMF three times and left in an oven overnight at 60 °C. Thus, CC grown with Co-MOF, Fe-MOF and Zn-MOF were formed. In order to examine the effects of reaction time and reactant concentration on the Co-MOF morphology, CC@Co-MOFs were fabricated according to the same procedures except that the reaction times were 15 min, 30 min, 60 min and 180 min, and two other reactants concentrations were 2:2 and 4:2. In order to confirm the phase transformation of CC@Co-MOF, it was calcinated in a furnace at 450 °C for 1 h in an Ar atmosphere.

2.3. Characterizations

The morphology of the products was characterized using field-emission scanning electron microscopy (TM-3000, Hitachi) and transmission electron microscopy (TEM; Jeol, JEM-2100F) at a 200-kV accelerating voltage. Energy dispersive X-ray spectroscopy (EDS) spectra of a MOF nanoflake were obtained from a scanning electron microscope (SEM; TESCAN VEGA3). X-ray photoelectron spectra (XPS) were recorded on a PHI 5000 VersaProbe 2 spectrometer. The wettability of epoxy on CC@Co-MOF and CC were compared through measuring the contact angles of epoxy/CC@Co-MOF and epoxy/CC. An X-ray diffractometer (XRD; Rigaku Smartlab 9 kW) was used to detect the phase purity of CC@Co_3O_4. Thermogravimetric analysis (TGA; TGA/DSC3 + [Mettler Toledo]) was used to measure the thermal properties of CC@Co-MOF.

In order to demonstrate the mechanical strength of Co-MOF nanoflakes, CC@Co-MOF reinforced polymer composites were fabricated using a wet layup method. After the epoxy resin was blended with a curing agent at a weight ratio of 100:27.2, CC@Co-MOF was fully saturated with resin and placed between two thin sheets of plastic. The excess resin was then squeezed out using a plastic scraper. A stainless-steel plate was cleaned and used as the base for the wet layup process, followed by the application of a releasing agent. Afterwards, symmetric laminates [(+45/−45/0/90/90/0/−45/+45)] were prepared by stacking together eight layers of CC@Co-MOF. The eight layers were then topped up with a breather fabric and perforated parting film. Finally, the whole set was covered with a bagging material, and a vacuum pump was used to provide differential pressure, which helped to wet the carbon fiber. All specimens were left to cure for 2 days without any post-curing. Afterwards, short beam strength (SBS) tests were carried out according to the standard test method ASTM D2344 using an electronic universal testing machine (WDW-10Y, Beijing United Test Co., Ltd.) under crosshead displacement control at a rate of 1 mm/min. After the SBS test, SEM images of the fractured samples and EDS plane scan and line scan analysis were also obtained with the TESCAN VEGA3. Furthermore, nanoindentation tests were used to determine the strength of polymer/Co-MOF nanoflakes interface. The sample was cut from the CC@Co-MOF reinforced polymer composites and the thickness was ~2 mm. The indentation tests were run in displacement-control mode using a maximum indentation depth of 80 nm. A trapezoidal load was applied in the nanoindentation testing. The indenter took 5 s to load the function, and the load was released within 5 s after being maintained for 10 s. The same procedures were carried out with CC reinforced polymer composites.

3. Results and discussion

3.1. Surface morphology and elemental composition of CC@CO-MOF nanoflakes

The synthesis procedures of CC@CO-MOF nanoflakes comprise three steps (Fig. 1a). First, CC was oxidized in concentrated acid to form CC-COOH. CO-MOF was then grown on CC-COOH due to the alternating growth of Co^{2+} and 2-methylimidazole through immersion in solution for 24 h. SEM characterizations clearly demonstrate the morphologic difference of three different kinds of CC. Axial grooves on the pristine CC (Fig. 1b and 1e) are visibly deepened after acidification (CC-COOH) (Fig. 1c and f). Unlike the chaotic coatings achieved without carboxylation [20], the carboxyl groups on the CC-COOH facilitate the formation of CO-MOF (Fig. 1d and g) via metal–carboxyl bonds [21,22]. According to the SEM images, the neighboring MOF nanoflakes form macropores with a dimension of ~200 nm. The low

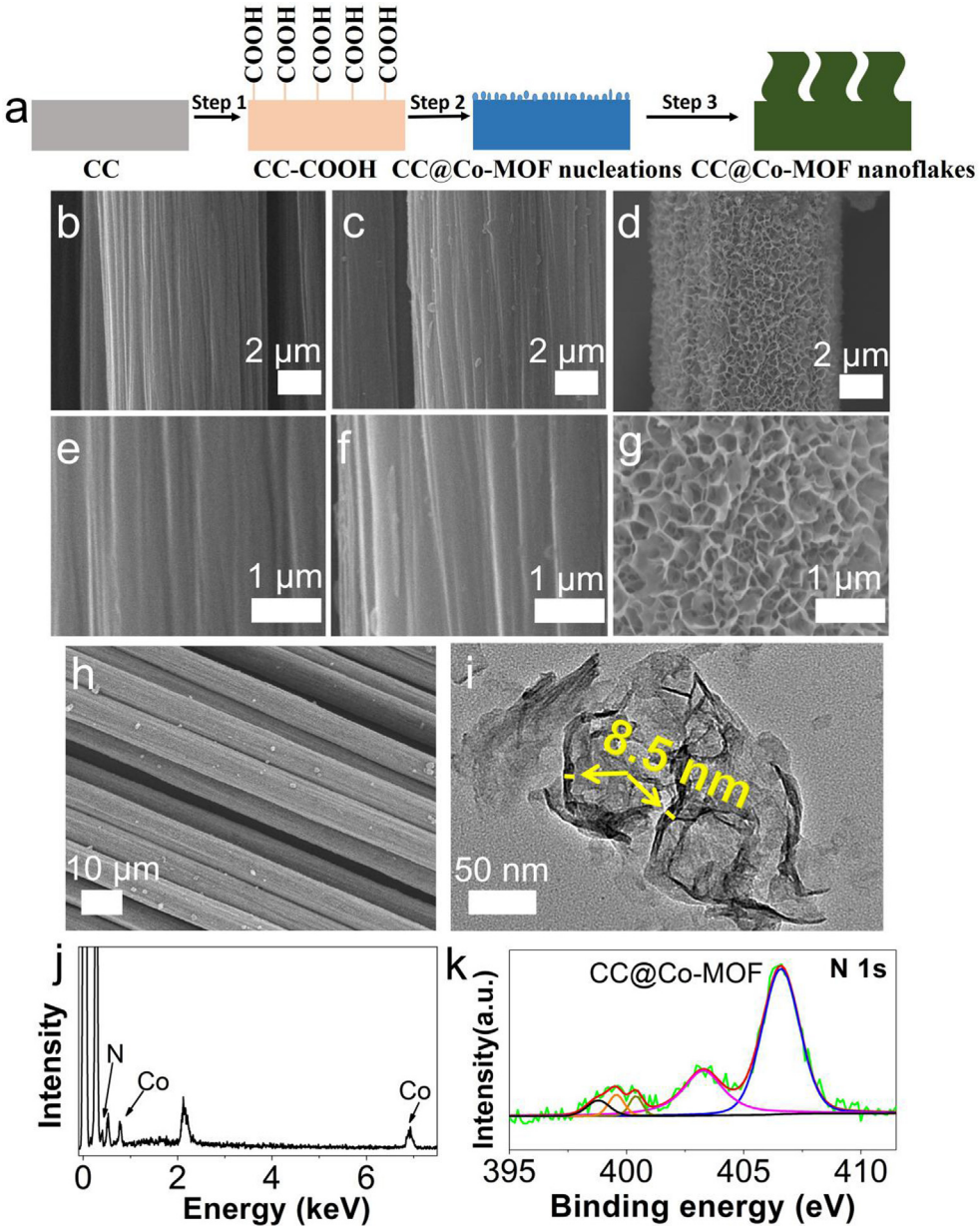

Fig. 1. (a) The synthesis procedures for CC@Co-MOF nanoflakes. SEM images of the surface morphologies of CC (b and e), CC-COOH (c and f) and CC@CO-MOF reacted for 24 h at the reactant concentration of 2:1 (d and g) at the magnifications of a, b, c: ×10 k; d, e, f: ×30 k. (h) A low-magnification SEM image of CC@Co-MOF. (i) A low-magnification TEM image of a CO-MOF nanoflake. (j) EDS spectrum for a CO-MOF nanoflake. (k) XPS spectra of CC@CO-MOF in N 1s. (For interpretation of the references to color in this figure legend, the reader is referred to the web version of this article.)

magnification SEM image (Fig. 1h) demonstrates a homogeneous MOF coating on the CC. In comparison, for the CC-COOH reacted in Zn $(NO_3)_2{\cdot}6H_2O$/2-methylimidazole DMF solution, few polygonal particles (Fig. S1a) was seen on a carbon fiber. Likewise, for the CC-COOH reacted in $FeCl_3$/1,4-Benzenedicarboxylic acid DMF solution, only low-density small particles (Fig. S1b) were seen on carbon fibers. Therefore, it is obvious that among the three kinds of precursor solutions, Co-based MOF precursor solution is superior to Zn-based and Fe-based MOF precursors in achieving the homogeneous modification of carbon fiber.

A TEM image (Fig. 1i) further confirms the flake structure of CO-MOF. The silk gauze-like morphology with transparent features indicates the ultrathin nature of the CO-MOF nanoflakes, consistent with the SEM results. The dark strips on the TEM image appeared due to the fact that one nanoflake was aslant or perpendicular to the substrate, from which the thickness of the nanoflake is measured to be 8.5 nm. EDS analysis (Fig. 1j) confirms the presence of Co and N in the MOF nanoflakes. The N 1s XPS spectrum (Fig. 1k) of CO-MOF is deconvoluted into five different component peaks, which can be assigned to pyridinic-like N (N1, ~398.1 eV) [23], pyrrolic-like N (N2, 400.3 eV), N coordinated with Co^{2+} in the CO-MOF framework (399.0 eV, Co–N), oxidized pyridinic-like N [24], and physically absorbed NO_3^- from the mixed methanol solution of $Co(NO_3)_2{\cdot}6H_2O$ and 2-methylimidazole [25].

3.2. Physical and mechanical properties of Co-MOF nanoflakes

Considering the growing interests in polymer-based catalysts [26–29] and batteries using solid state polymer electrolytes [30–32], the materials which have high potential to be used as catalysts or electrode materials need to be examined to confirm their compatibility with polymer. Herein, epoxy, as a kind of polymer which has good adhesion, low shrinkage, high tensile strength and modulus, and good

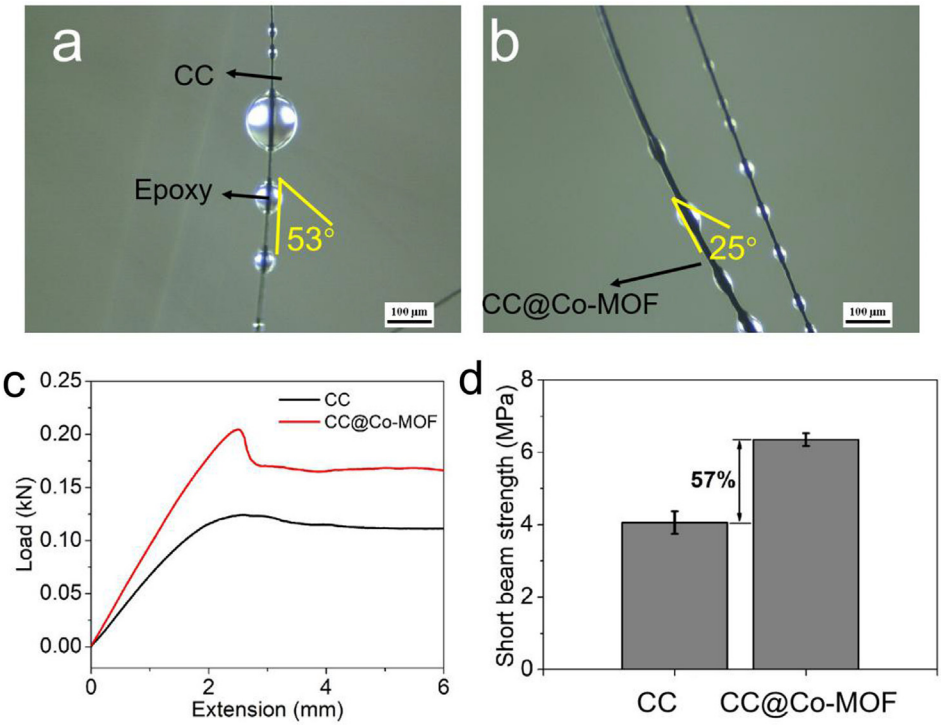

Fig. 2. Optical images of contact angles of micro-droplets of epoxy on (a) CC and (b) CC@CO-MOF. (c) Load vs. extension graphs of the SBS tests for CC and CC@CO-MOF reinforced polymer composites. (d) Comparison of SBS strength values of the two kinds of reinforced polymer composites. (For interpretation of the references to color in this figure legend, the reader is referred to the web version of this article.)

chemical and corrosion resistance, was used to examine the wettability of polymer on CC@Co-MOF. When a micro-drop of epoxy resin was applied on single carbon fibers, the contact angle of epoxy on CC@Co-MOF fiber is only 25°, significantly lower than that on carbon fiber (53°) (Fig. 2a and b), demonstrating the better wettability of polymer on the modified CC. The measurement of the contact angles of epoxy on CC and CC@Co-MOF was based on the selection of two microdroplets of the same size. Therefore, it can be seen that CC@Co-MOF has better polymer compatibility compared to CC.

In order to know about the strength of Co-MOF nanoflakes, SBS testing was performed to measure the mechanical strength of the CC@Co-MOF nanoflakes reinforced polymer composites. Fig. 2c shows typical load–extension curves of two sets of SBS tests for two kinds of CC-based polymer. As shown in Fig. 2d, CC@CO-MOF reinforced polymer composites has a short beam strength of 6.35 MPa, which is ~60% higher compared to CC reinforced polymer composites. According to the SEM images (Fig. 1), the Co-MOF nanoflakes have three-dimensional (3D) ordered and macroporous structures, which can significantly increase the contact area between the polymer and the fiber. Thus, when the polymer infiltrates the modified carbon fibers, mechanical interlocking is introduced between the carbon fibers and the polymer. Based on the uniform growth of Co-MOF nanoflakes on the carbon fibers, every carbon fiber contributes efficiently to load transfer from the polymer to the fiber, which helps to achieve the enhancement in the SBS strength. However, the enhanced SBS strength could not be achieved unless Co-MOF nanoflakes are mechanically strong and cannot be easily broken. Therefore, the strength of Co-MOF nanoflakes is demonstrated. To confirm the mechanical interlocking effect between polymer and CC facilitated by the Co-MOF nanoflakes, the fractured surfaces after the SBS tests were examined by SEM. Fig. 3a shows that a larger amount of polymer is retained on the surface of CC@CO-MOF fibers than that on CC fibers (Fig. S2a) due to the difficulty of polymer in debonding from CC@CO-MOF fibers. The accurate chemical composition of the fractured surface of CC@CO-MOF reinforced polymer composites was detected by taking EDS elemental mapping [33,34] images of the polymer (Fig. 3c) bonded onto a CC@Co-MOF fiber. According to the images (Fig. 3d–f), Co, C, and O coexisted in the fractured area, suggesting the presence of embedded MOF nanoflakes in

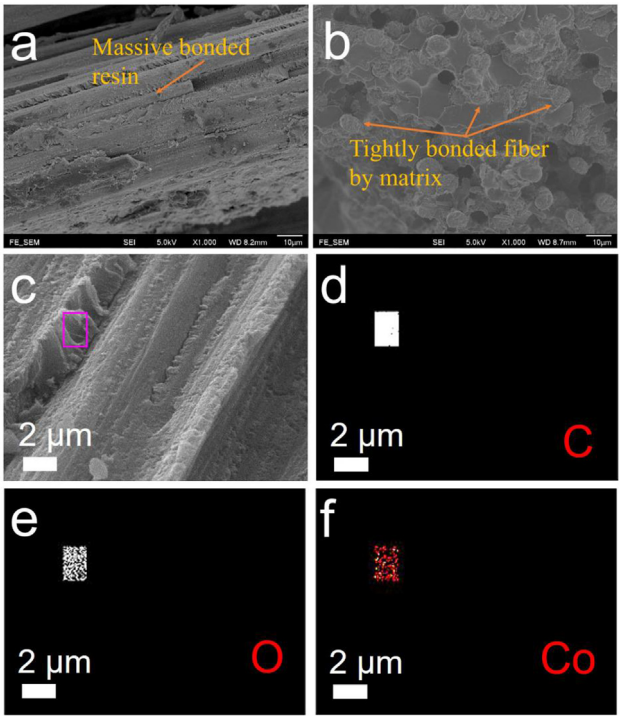

Fig. 3. (a and b) SEM micrographs of the fractured surface of CC@CO-MOF reinforced polymer composites. (c–f) A representative plane scan SEM image of the fractured surfaces of CC@Co-MOF reinforced polymer composites at the magnification of ×1000 and corresponding EDS plane scan mapping images. (For interpretation of the references to color in this figure legend, the reader is referred to the web version of this article.)

the polymer. The EDS line scan along the yellow line (Fig. S3a–d) also demonstrates the existence of MOF nanoflakes oriented parallel to the axis of the carbon fiber and the successful wrapping by polymer. Therefore, the polymer compatibility and wettability of polymer on CC@Co-MOF are confirmed again. Lastly, due to mechanical

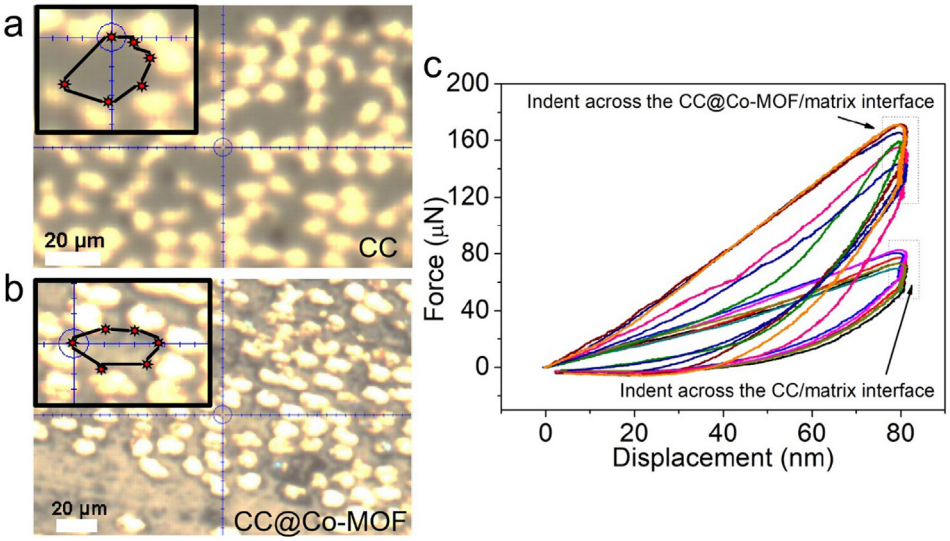

Fig. 4. (a) Optical microscopic image showing the region selected for nanoindentation studies across the interface of the CC reinforced polymer composites. (b) Optical microscopic image showing the region selected for nanoindentation studies across the interface of the CC@Co-MOF reinforced polymer composites. (c) Comparison of the force–displacement curves for the nanoindentations made on both the CC and CC@Co-MOF reinforced polymer composites. (For interpretation of the references to color in this figure legend, the reader is referred to the web version of this article.)

interlocking, the tight bonding on the polymer-fiber interface makes fiber pull-out more difficult, therefore, no obvious gaps between the polymer and the fiber are observable in CC@Co-MOF reinforced polymer composites (Fig. 3b) while large gaps are observed in CC reinforced polymer composites (Fig. S2b), which also help to demonstrate the strength of Co-MOF nanoflakes. Otherwise, the stress at which Co-MOF nanoflakes break would be lower than that at fiber pull-out, thus resulting in a lower SBS strength. In summary, the SEM micrographs of the fractured surfaces and the EDS element analysis collectively verify the mechanical interlocking effect between the modified CC and polymer through Co-MOF nanoflakes.

Now the mechanical strength of the Co-MOF nanoflake and its compatibility with polymer have both been proved, the interphase of CC@Co-MOF/polymer also need to be considered. For the nanocomposites, an interphase is formed at the contact area of two kinds of materials, which can have a significant effect on the properties of nanocomposites. Nanoindentation testing is a representative method to measure the strength of the interphase. A Berkovich indenter was used to indent the near-fiber region of the polymer to determine the nanomechanical properties of the interphase. Fig. 4 shows optical microscopic images of the CC/CC@Co-MOF reinforced polymer composites, including the selected regions for nanoindentation. The regions of interest included one region of polymer surrounded by several carbon fibers. The red spots on the images of Fig. 4a and b represent the nanoindentation points made across the interfaces of the CC and CC@Co-MOF reinforced polymer composites, respectively. Fig. 4c illustrates force–displacement curves for all indentations. According to Fig. 4c, due to the in-situ grown Co-MOF nanoflakes, the strength of interphase of CC@Co-MOF reinforced polymer composites experiences a significant increase (90% at maximum) compared to CC reinforced polymer composites. The gradual variation in force from polymer to carbon fiber across the MOF nanoflakes-incorporated interphase can more effectively suppress the unwanted stress concentrations around the carbon fiber, thus demonstrating remarkably enhanced load-bearing capacity of the polymer-based composites. Therefore, the newly designed ultrathin Co-MOF nanoflakes are not only blessed with inherent mechanical strength but are also expected to obtain a strong interphase in polymer-based products.

3.3. Future research directions of CC@Co-MOF

MOFs are generally used as templates to derive metal oxides. MOF nanoflakes, capable of retaining pristine microstructures after pyrolysis [16,17,35], offer a facile route to obtain functional materials with various applications. In order to explore the high potential of CC@Co-MOF for future applications, phase transformation from Co-MOF to Co_3O_4 and the capability of Co_3O_4 to inherit the structure of MOF after pyrolysis need to be confirmed. Thermal properties of CC@Co-MOF were investigated. According to the TGA curve in Fig. 5a, weight loss first happened at ~250 °C due to the release of organic linkers. As the temperature increased, the weight loss was gradually accelerated. The surface morphology of CC@Co-MOF calcinated at 450 °C was examined by SEM. The temperature was chosen since it was widely used as the pyrolysis temperature of Co-based MOF to produce cobalt oxide. According to the SEM image (Fig. 5b), the nanoflake structure of Co-MOF was well maintained after pyrolysis. The calcinated CC@Co-MOF were further investigated by XRD to confirm the exact phase compositions of the carbonized products on the carbon fibers. By comparing the XRD spectrum (Fig. 5c) with the JCPDS cards, the peaks in the XRD spectrum are all identical to JCPDS card No. 00-09-0418, except for the two peaks from graphitic carbon, which further confirms the formation of Co_3O_4. Therefore, the phase transformation from CC@Co-MOF to CC@Co_3O_4 was successfully confirmed and broader applications of this newly designed CC@Co-MOF nanoflakes can be explored [36,37].

Now that the phase transformation of Co-MOF to Co_3O_4 has been confirmed, parameters affecting the growth of CC@Co-MOF nanoflakes were investigated to achieve good control of the morphology of CC@Co_3O_4. The detailed growth process of Co-MOF on CC based on the combination of Co^{2+} and 2-methylimidazole has been explored by SEM characterizations. By observing the morphology change of the CC-COOH after incubation in $Co(NO_3)_2{\cdot}6H_2O$ and 2-methylimidazole methanol solution for different time periods of 15 min, 30 min, 60 min, and 180 min, the effect of reaction time on the growth of Co-MOF nanoflakes was examined (Fig. 6). At 15 min, only particles can be seen in the surface grooves of carbon fibers (Fig. 6a), which indicates the nucleation of some crystals, as shown in the schematic in Fig. 6a. At 30 min, some rugged structures have emerged on the surface of carbon fibers (Fig. 6b). However, the carbon fiber surface are still exposed. At 60 min, the carbon fiber surface is totally covered by the Co-MOF nanoflake (Fig. 6c). By 180 min (Fig. 6d), the nanoflake structures have become very dense, and some silk gauze-like structures have emerged, indicating the ultrathin characteristics of the MOF nanoflakes. It is very interesting to find that density and length of these ultrathin nanoflakes can be easily controlled by changing the growth time. Interestingly, Liang et al[16] has reported the growth of MOF nanoflakes on a nickel foam. However, unlike the fast MOF nucleation over the whole nickel foam surface within 2 min, there appear only discrete particles on carbon fiber surface after 15 min, which shows more sluggish kinetics

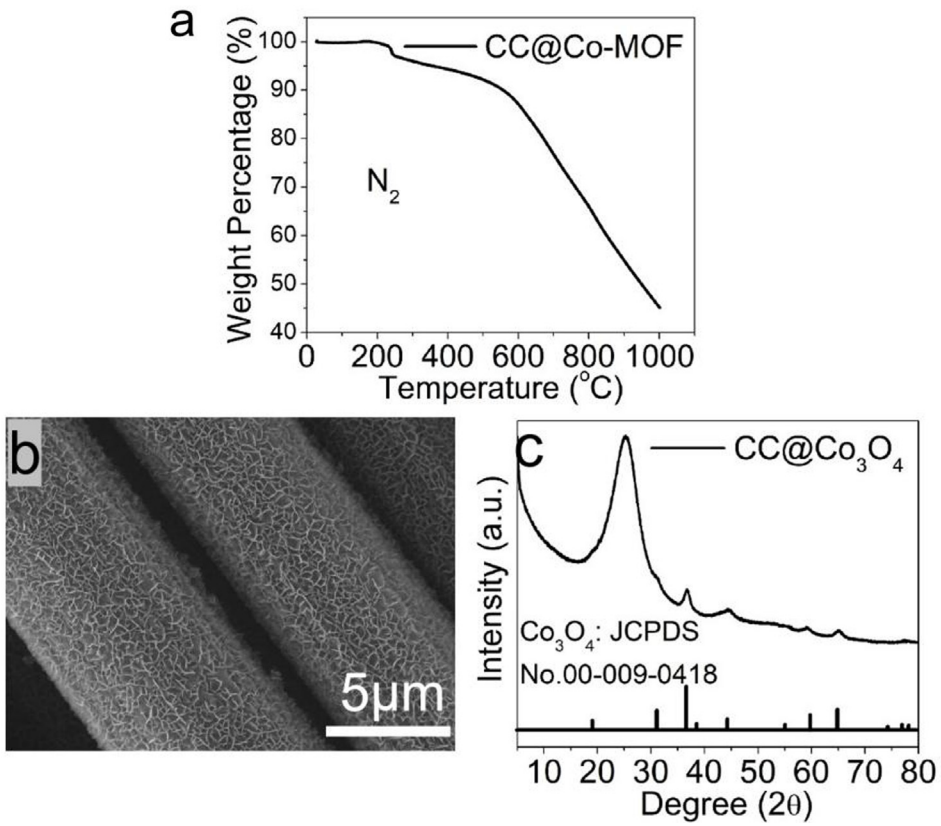

Fig. 5. (a) A TGA curve of CC@Co-MOF. (b) A SEM image of CC@Co_3O_4. (c) A XRD spectrum of CC@Co_3O_4.

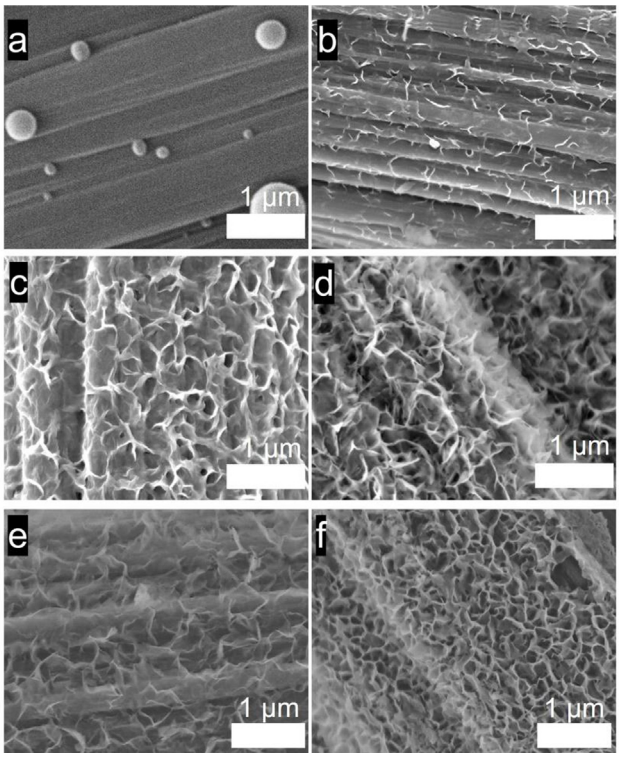

Fig. 6. SEM images of the surface morphology of CC@Co-MOF at various incubation times: (a) 15 min, (b) 30 min, (c) 60 min, (d) 180 min with a constant reactant concentration of 2:1, and at two other reactant concentrations of 4:2 (e) and 2:2 (f) with a constant reaction time of 24 h at the magnification of ×30 k.

of carbon fiber for the initiation of MOF growth. Whether and how this kinetic difference affects the growth and the property of substrate-based MOF will be our future work. In order to better understand the formation of Co-MOF on carbon fiber, two other reactant concentrations (molar ratios of $Co(NO_3)_2{\cdot}6H_2O$ and 2-methylimidazole = 2:2 and 4:2) were used to examine the effect of reactants concentration on Co-MOF morphology. Through comparing the Co-MOF morphology obtained at the reactants concentration of 4:2 (Fig. 6e) with 2:1, it can be found that despite the same molar ratio of $Co(NO_3)_2{\cdot}6H_2O$ and 2-methylimidazole, a higher reactant concentration can bring about significantly different Co-MOF morphology. Instead of approximately hexagonal macropores formed by neighboring Co-MOF nanoflakes at the concentration of 2:1, the concentration of 4:2 facilitates the growth of seemingly randomly packed Co-MOF nanoflakes on carbon fibers. In contrast, even though approximately hexagonal macropores are formed, a higher 2-methylimidazole concentration (2:2) is conductive to the formation of smaller macropores (Fig. 6f) with a dimension of ~100 nm. Therefore, reactants concentration plays an important role in the morphology control of CC@Co-MOF nanoflakes. In summary, studying Co-MOF growth with time period and reactants concentration enables us to get a clue on how to tune the morphology of Co-MOF. Different time periods and reactants concentrations result in distinctive Co-MOF densities which can in turn determine the mass loading of Co_3O_4. Based on this, it is possible for us to easily control the morphology of Co_3O_4 and tailor it to the applications of catalysts and batteries.

Now future research areas can be proposed. In terms of the application of CC@Co_3O_4 nanoflakes for electrocatalysis, the formation of MOF-derived defect-abundant metal oxide electrocatalysts is a promising strategy for the enhancement of electrochemical performances. Especially, the nanometre thicknesses of ultrathin Co_3O_4 nanoflakes allow superior electron transfer and rapid mass transport. Besides, extremely high percentages of exposed catalytic active surfaces can

ensure high catalytic activity. As a result, making Co_3O_4 nanoflakes ultrathin will facilitate the discovery of CC-based Co_3O_4 catalysts with outstanding catalytic properties. For the application of CC@Co_3O_4 nanoflakes for batteries, the low electrical conductivity of Co_3O_4 combined with 3D electro-conductive carbon fibers can gain the maximum efficiencies. Besides, due to the ultrathin structures of Co_3O_4, CC@Co_3O_4 not only possesses large surface areas with the maximum exposure of active sites for electrochemical reactions, but is also blessed with a short Li ion diffusion length, which affords a high possibility to obtain CC-based electrodes with outstanding electrochemical properties. Therefore, the successful fabrication of CC@ultrathin Co_3O_4 nanoflakes affords a high probability of discovery of promising catalysts and electrodes for energy storage devices.

In addition, the practicability of CC@Co_3O_4 as electrodes for solid state batteries, such as composite structural battery can also be examined. For solid-state batteries incorporating metal oxide active materials and solid state polymer electrolytes [38,39], one very important issue is the polymer electrolyte/electrode interface. From an electrochemical perspective, most of active materials in situ grown on CC suffer from significant volume expansion [40] when subjected to lithiation/delithiation, which will generate stresses at the polymer/CC interface [41]. Especially, when the polymer/CC interface suffers from cyclic volume expansion/contraction, the interface may be destroyed. From an mechanical perspective, when active materials grown on CC are not undergoing electrochemical reactions, the mechanical interlocking effect facilitated by active materials may contribute to the enhancement of interfacial adhesion between CC and polymer electrolyte. However, once lithiation of active materials brings about volume expansion, the stress induced by volume expansion may form stress concentration points, leading to the breakage of the polymer electrolyte/CC interface. Thus, the volume expansion of the active materials at the CC/polymer interface plays an significant role in the mechanical and electrochemical stability of solid state batteries. For the CC@ultrathin Co_3O_4 nanoflakes obtained in this study, ultrathin and morphology-controllable structures make it possible to obtain Co_3O_4 active materials with small volume expansion, which will have limited effect on the polymer/CC interface. Thus, the successful fabrication of CC@Co_3O_4 can also afford a high probability of discovery of promising electrodes for solid-state energy storage devices which can simultaneously achieve electrochemical and mechanical stabilities. This will lay foundations for the fabrication of next-generation CC-reinforced polymer composites with multifunctional performances such as energy storage.

4. Conclusions

A facile method for the in-situ synthesis of ultrathin and mechanically strong macroporous MOF nanoflakes on CC is demonstrated. CC grown with CO-MOFs is easily fabricated by acidification and subsequent hydrothermal reaction. The roles of reaction time and reactants concentration in the easy control of the Co-MOF morphology have been demonstrated. For future research directions, the phase transformation from Co-MOF to Co_3O_4 and the preserved ultrathin structure make it attractive to investigate the potential of CC@Co_3O_4 nanoflakes as electrocatalysts in electrochemical conversion technologies and electrodes in energy storage devices. Furthermore, the research on simultaneous achievement of mechanical and electrochemical stability of composite structural batteries through incorporation of volume-expansion-controllable CC@Co_3O_4 electrodes is put forward. Therefore, the newly designed CC supported ultrathin MOF nanoflakes not only enriches the family of MOFs but lays the foundation for realizing next-generation CC-reinforced polymer composites with multifunctional performances.

CRediT authorship contribution statement

Yu Fu: Conceptualization, Methodology , Investigation, Writing - original draft. **Hanmo Zhou:** Writing - review & editing. **Sha Yin:** Writing - review & editing. **Limin Zhou:** Conceptualization, Funding acquisition.

Declaration of Competing Interest

The authors declare that they have no known competing financial interests or personal relationships that could have appeared to influence the work reported in this paper.

Acknowledgements

This work was financially supported by The Hong Kong Polytechnic University (grants: 1-ZVJD and RKC7). The authors are also thankful for the technical support provided by Composites & Fabrication Stream in Industrial Centre of The Hong Kong Polytechnic University.

Appendix A. Supplementary material

Supplementary data to this article can be found online at https://doi.org/10.1016/j.compositesa.2020.105910.

References

[1] Yaghi OM, O'Keeffe M, Ockwig NW, Chae HK, Eddaoudi M, Kim J. Reticular synthesis and the design of new materials. Nature 2003;423(6941):705–14.
[2] Furukawa H, Cordova KE, O'Keeffe M, Yaghi OM. The chemistry and applications of metal-organic frameworks. Science 2013;341(6149):1230444.
[3] Kuyuldar S, Genna DT, Burda C. On the potential for nanoscale metal–organic frameworks for energy applications. J Mater Chem A 2019;7(38):21545–76.
[4] Lu M, Li Y, He P, Cong J, Chen D, Wang J, et al. Bimetallic metal-organic framework nanosheets as efficient electrocatalysts for oxygen evolution reaction. J Solid State Chem 2019;272:32–7.
[5] Ma K, Wang Y, Chen Z, Islamoglu T, Lai C, Wang X, et al. Facile and scalable coating of metal-organic frameworks on fibrous substrates by a coordination replication method at room temperature. ACS Appl Mater Interfaces 2019;11(25):22714–21.
[6] Ma J, Li J, Guo R, Xu H, Shi F, Dang L, et al. Direct growth of flake-like metal-organic framework on textile carbon cloth as high-performance supercapacitor electrode. J Power Sources 2019;428:124–30.
[7] Liu Q, Xie L, Shi X, Du G, Asiri AM, Luo Y, et al. High-performance water oxidation electrocatalysis enabled by a Ni-MOF nanosheet array. Inorg Chem Front 2018;5(7):1570–4.
[8] Li Y, Xie M, Zhang X, Liu Q, Lin D, Xu C, et al. Co-MOF nanosheet array: A high-performance electrochemical sensor for non-enzymatic glucose detection. Sensor Actuat B-Chem 2019;278:126–32.
[9] Yang T, Song TT, Callsen M, Zhou J, Chai JW, Feng YP, et al. Atomically thin 2D transition metal oxides: structural reconstruction, interaction with substrates, and potential applications. Adv Mater Interfaces 2019;6(1):1801160.
[10] Zhang Q, Zhou Z, Pan Z, Sun J, He B, Li Q, et al. All-metal-organic framework-derived battery materials on carbon nanotube fibers for wearable energy-storage device. Adv Sci 2018;5(12):1801462. https://doi.org/10.1002/advs.v5.1210.1002/advs.201801462.
[11] Zhao S, Wang Y, Dong J, He C-T, Yin H, An P, et al. Ultrathin metal–organic framework nanosheets for electrocatalytic oxygen evolution. Nat Energy 2016;1(12):16184.
[12] Zhu Y, Cao C, Zhang J, Xu X. Two-dimensional ultrathin $ZnCo_2O_4$ nanosheets: general formation and lithium storage application. J Mater Chem A 2015;3(18):9556–64.
[13] Nian P, Liu H, Zhang X. Bottom-up synthesis of 2D Co-based metal–organic framework nanosheets by an ammonia-assisted strategy for tuning the crystal morphology. CrystEngComm 2019;21(20):3199–208.
[14] Zhuang JL, Terfort A, Woll C. Formation of oriented and patterned films of metal-organic frameworks by liquid phase epitaxy: A review. Coordin Chem Rev 2016;307:391–424.
[15] Mei J, Liao T, Ayoko GA, Bell J, Sun Z. Cobalt oxide-based nanoarchitectures for electrochemical energy applications. Prog Mater Sci 2019;103:596–677.
[16] Fang G, Zhou J, Liang C, Pan A, Zhang C, Tang Y, et al. MOFs nanosheets derived porous metal oxide-coated three-dimensional substrates for lithium-ion battery applications. Nano Energy 2016;26:57–65.
[17] Xu D, Chao D, Wang H, Gong Y, Wang R, He B, et al. Flexible quasi-solid-state sodium-ion capacitors developed using 2D metal–organic-framework array as reactor. Adv Energy Mater 2018;8(13):1702769.
[18] Guan C, Sumboja A, Wu H, Ren W, Liu X, Zhang H, et al. Hollow Co_3O_4 nanosphere embedded in carbon arrays for stable and flexible solid-state zinc-air batteries. Adv

Mater 2017;29(44):1704117.
[19] Chen W, Han B, Tian C, Liu X, Liang S, Deng H, et al. MOFs-derived ultrathin holey Co_3O_4 nanosheets for enhanced visible light CO_2 reduction. Appl Catal B 2019;244:996–1003. https://doi.org/10.1016/j.apcatb.2018.12.045.
[20] Yang X, Jiang X, Huang Y, Guo Z, Shao L. Building nanoporous metal-organic frameworks "armor" on fibers for high-performance composite materials. ACS Appl Mater Interfaces 2017;9(6):5590–9.
[21] Bradshaw D, Garai A, Huo J. Metal-organic framework growth at functional interfaces: thin films and composites for diverse applications. Chem Soc Rev 2012;41(6):2344–81.
[22] Falcaro P, Ricco R, Doherty CM, Liang K, Hill AJ, Styles MJ. MOF positioning technology and device fabrication. Chem Soc Rev 2014;43(16):5513–60.
[23] He W, Ifraemov R, Raslin A, Hod I. Room-temperature electrochemical conversion of metal-organic frameworks into porous amorphous metal sulfides with tailored composition and hydrogen evolution activity. Adv Funct Mater 2018;28(18):1707244.
[24] Tai J, Hu J, Chen Z, Lu H. Two-step synthesis of boron and nitrogen co-doped graphene as a synergistically enhanced catalyst for the oxygen reduction reaction. RSC Adv 2014;4(106):61437–43.
[25] Křepelová A, Newberg J, Huthwelker T, Bluhm H, Ammann M. The nature of nitrate at the ice surface studied by XPS and NEXAFS. Phys Chem Chem Phys 2010;12(31):8870–80.
[26] Poupart R, Grande D, Carbonnier B, Le Droumaguet B. Porous polymers and metallic nanoparticles: A hybrid wedding as a robust method toward efficient supported catalytic systems. Prog Polym Sci 2019;96:21–42.
[27] Nasrollahzadeh M, Sajjadi M, Shokouhimehr M, Varma RS. Recent developments in palladium (nano)catalysts supported on polymers for selective and sustainable oxidation processes. Coordin Chem Rev 2019;397:54–75.
[28] Howard IC, Hammond C, Buchard A. Polymer-supported metal catalysts for the heterogeneous polymerisation of lactones. Polym Chem 2019;10(43):5894–904.
[29] Mujahed S, Valentini F, Cohen S, Vaccaro L, Gelman D. Polymer-anchored bifunctional pincer catalysts for chemoselective transfer hydrogenation and related reactions. ChemSusChem 2019;12(20):4693–9.
[30] Chen R, Qu W, Guo X, Li L, Wu F. The pursuit of solid-state electrolytes for lithium batteries: from comprehensive insight to emerging horizons. Mater Horiz 2016;3(6):487–516.
[31] Janek J, Zeier WG. A solid future for battery development. Nat Energy 2016;1(9). https://doi.org/10.1038/nenergy.2016.141.
[32] Muldoon J, Bucur CB, Boaretto N, Gregory T, di Noto V. Polymers: Opening doors to future batteries. Polym Rev 2015;55(2):208–46.
[33] Han Y, Shi X, Yang X, Guo Y, Zhang J, Kong J, et al. Enhanced thermal conductivities of epoxy nanocomposites via incorporating in-situ fabricated hetero-structured SiC-BNNS fillers. Compos Sci Technol 2020;187:107944.
[34] Zhang R-H, Shi X-T, Tang L, Liu Z, Zhang J-L, Guo Y-Q, et al. Thermally conductive and insulating epoxy composites by synchronously incorporating Si-sol functionalized glass fibers and boron nitride fillers. Chinese J Polym Sci 2020. https://doi.org/10.1007/s10118-020-2391-0.
[35] Wei GJ, Zhou Z, Zhao XX, Zhang WQ, An CH. Ultrathin metal-organic framework nanosheet-derived ultrathin Co_3O_4 nanomeshes with robust oxygen-evolving performance and asymmetric supercapacitors. ACS Appl Mater Interfaces 2018;10(28):23721–30.
[36] Chen Y-Z, Zhang R, Jiao L, Jiang H-L. Metal–organic framework-derived porous materials for catalysis. Coordin Chem Rev 2018;362:1–23.
[37] Cao X, Tan C, Sindoro M, Zhang H. Hybrid micro-/nano-structures derived from metal–organic frameworks: preparation and applications in energy storage and conversion. Chem Soc Rev 2017;46(10):2660–77.
[38] Zhou GM, Li F, Cheng HM. Progress in flexible lithium batteries and future prospects. Energy Environ Sci 2014;7(4):1307–38.
[39] Liu Y, Sun ZH, Tan K, Denis DK, Sun JF, Liang LW, et al. Recent progress in flexible non-lithium based rechargeable batteries. J Mater Chem A 2019;7(9):4353–82.
[40] Eftekhari A. Low voltage anode materials for lithium-ion batteries. Energy Stor Mater 2017;7:157–80.
[41] Peryez SA, Cambaz MA, Thangadurai V, Fichtnert M. Interface in solid-state lithium battery: challenges, progress, and outlook. ACS Appl Mater Interfaces 2019;11(25):22029–50.